J. Coat. Technol. Res., **7** (5) 623–635, 2010
DOI 10.1007/s11998-010-9242-9

On the stress distribution at scratching of thin film structures

Fredrik Wredenberg, Per-Lennart Larsson

Abstract Scratching of thin film/substrate structures is studied theoretically and numerically. In most cases, the material behavior of the film as well as the substrate is described by classical elastoplasticity accounting for large deformations; further, pressure-sensitive flow models are considered. The main efforts are devoted toward an understanding of the influence from the film/substrate boundary on the stress distribution at scratching but for comparative reasons, scratching of homogeneous materials are also studied and pertinent results presented. Among other things, the results are discussed in relation to delamination initiation and growth at scratching. The numerical investigation is performed using the finite element method, and the numerical strategy is discussed in some detail. The most important finding given by the present study is that high shear stresses are the main driving force for delamination initiation and growth along the film/substrate interface. It was also noted that the influence from pressure-sensitive flow on the stress fields related to delamination initiation is small, both quantitatively and qualitatively.

Keywords Scratching, Film/substrate structures, Stress distribution, FEM analysis, Delamination

F. Wredenberg, P.-L. Larsson (✉)
Department of Solid Mechanics, Royal Institute of Technology, 10044 Stockholm, Sweden
e-mail: pelle@hallf.kth.se

Present Address:
F. Wredenberg
Scania CV AB, 151 87 Södertälje, Sweden

Introduction

It is a well-known fact that microindentation provides information about elastic and plastic deformation on a localized scale, and it is particularly attractive for thin films with a typical thickness of a few micrometers or less. The commonly determined properties using microindentation are indentation hardness and the indentation load versus indentation depth curve. The indentation hardness represents a measure of the average pressure under the indenter tip and is calculated from the force necessary to push a rigid indenter into the material. An additional important parameter involved in the hardness calculation is the actual area of contact between the indenter and the material, usually estimated using suitable assumptions.

The values obtained during an indentation test are used to determine the constitutive properties of the materials, with the early theoretical studies by Sneddon,[1] Tabor,[2] and Johnson[3] being the most notable for this purpose. Depending on the material properties and the type of indenter used, Johnson[3] suggested that the outcome of a sharp indentation test on classical elastoplastic materials could be placed in one of three levels as specified by the parameter

$$\Lambda = E \tan\beta/\left((1-\nu^2)\sigma_{\text{rep}}\right). \quad (1)$$

In equation (1), E is the Young's modulus, ν is Poisson's ratio, β is the angle between the (sharp) indenter and the undeformed surface, and σ_{rep} is the material flow stress at a representative value of the effective (accumulated) plastic strain ε_{p}, chosen here as $\varepsilon_{\text{p}} = 0.08$. As for the three indentation levels, schematically shown in Fig. 1, Level I, $\Lambda < 3$, corresponds to the occurrence of very little plastic deformation during indentation testing, meaning that all global properties can be derived from an elastic analysis. In level II, $3 < \Lambda < 30$, an increasing amount of plastic deformation

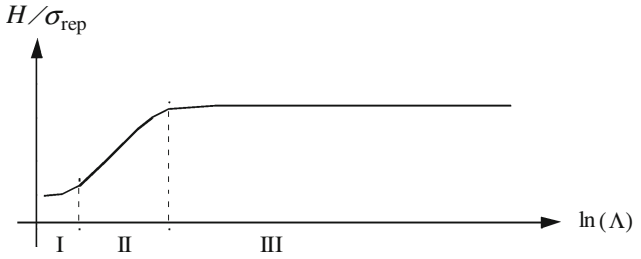

Fig. 1: Sketch of the characteristic behavior at indentation.[3] The indentation hardness *H* divided by the representative stress σ_{rep} is plotted against the nondimensional strain parameter Λ

is present, and both the elastic and plastic properties of the material will influence the outcome of the test, and finally, in level III, $\Lambda > 30$, plastic deformation is present over the entire contact area. The last mentioned level is applicable to most engineering metals. From a number of tests performed on different materials pertinent to level III, Tabor[2] concluded that a simple formula relating hardness, flow stress, and a constant dependent on the geometry of the sharp indenter could be derived. Although Tabor's method is basically empirical, since the complex stress distribution at elastoplastic indentation rules out an analytically based relation, it is known to give good accuracy in a number of cases. In this context, it should be mentioned that indentation testing is also frequently used to determine the elastic modulus of a material. Indeed, related study by Oliver and Pharr[4] now forms the basis for industrial standards regarding this feature.

As much as indentation testing has been used, few theoretical methods are available for the study of thin film indentation. Analytical methods can at best be used for studying elastic indentation of thin films, but at elastoplastic indentation it is necessary to use more advanced methods. Accordingly, given the complexity of such an indentation analysis, numerical methods like the finite element method (FEM) are, together with scaling and dimensional analysis as outlined by Cheng and Cheng,[5] often necessary tools for determining relevant quantities in an accurate manner. The early studies by Bhattachharya and Nix,[6,7] Laursen and Simo,[8] and Giannakopoulos and coworkers[9–12] demonstrated the usefulness of modeling a typical sharp indentation test using FEM and obtaining relevant values on, for example, the hardness in the case of bulk and thin film-type samples. Furthermore, as regards to sharp indentation, many authors reported on finite element studies performed on several thin film and substrate combinations, cf. e.g., reference (13–16) and, perhaps more generally, in reference (17). It should be noted in passing that many of these FEM studies of thin film indentation were inspired by the development of the nanoindenter.[18]

Nowadays, also scratch testing is a well-established technique for hardness testing. The fundamental

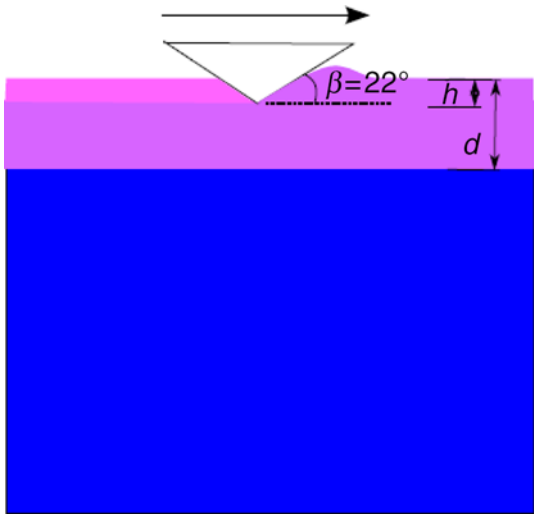

Fig. 2: Scratching of a film/substrate composite system where the angle *β* defines the geometry of the conical stylus

knowledge about the mechanical behavior at scratching is not nearly as developed as for indentation testing. Some early mechanical analyses concerning different aspects of scratching of metals should be mentioned though.[19–22] However, due to the complexity of the boundary value problem, the analysis of this type of hardness testing also requires numerical methods; again, FEM is to be preferred for a high accuracy analysis. In recent years, a number of such analyses have been presented, cf. e.g., references (23–25) with the most important conclusion being that the Johnson parameter in equation (1) can be used to correlate scratching experiments. Also thin film scratching has been studied quite frequently, cf. e.g., references (26–34) considering different aspects of the problem such as fracture, delamination, and the behavior of different global (and to some extent also local) scratch variables (global scratch variables include normal and tangential hardness, apparent coefficient of friction, and contact area).

A solid understanding of the mechanics at thin film scratching requires detailed knowledge of the local stress fields in such a situation. As indicated above, such an analysis has not been undertaken in full previously and the present aim is to remedy this shortcoming. In doing so, the numerical strategy, based on the FEM, developed by Wredenberg and Larsson,[24,25] was used while modified to also account for film/substrate boundary effects. Most of the numerical results are pertinent to standard elastoplastic material behavior, but pressure-sensitive Drucker–Prager plasticity[35] is also considered. In the latter case, the numerical implications have been discussed in detail by Wredenberg and Larsson.[33,36] For clarity and convenience, but not out of necessity, the analysis was restricted to cone scratching ($\beta = 22°$ in Fig. 2) of elastoplastic materials, as in such a case the indenter

does not introduce any characteristic length in the problem. In this context, it should be mentioned that $\beta = 22°$ was chosen as being a representative value for most sharp indenter geometries of practical interest. Furthermore, only soft homogeneous coatings are considered, and accordingly, the deformation of the substrate is neglected in the analysis. The present results, of course, then cannot be extended to coating systems with hard/nonhomogeneous coatings. However, in case of hard or, more correctly, harder coatings, some guidance is given in reference (34) as regards to the validity of the assumption of a stiff substrate.

Basic considerations and numerical analysis

The present analysis concerns scratching of thin film/substrate systems using a sharp conical stylus assumed to be rigid. It is assumed that quasi-static conditions do prevail. In the presentation below, h is the scratch depth and d is the film thickness, as shown in Fig. 2 and A is the normally projected contact area between stylus and material. Assuming that quasi-static and steady-state conditions prevail, the monolithic scratch problem is self-similar with no characteristic length present. Consequently, scratch hardness as well as the ratio $h/\sqrt{A}$ are constant during the loading sequence of a scratch test on homogeneous materials, and stresses and strains are functions of the dimensionless variables $x_i/\sqrt{A}$ and material properties alone. Presently, x_i is the base vector of a Cartesian coordinate system, following the stylus, with x_1 directed transverse to the scratch direction, x_2 directed along the scratch direction, and x_3 directed normal to the specimen surface (note that in the presentation of the results below the notation is $x_1 = x$, $x_2 = y$, $x_3 = z$). At scratching (or normal indentation) of thin film/substrate systems, this is of course not the case at increasing load as the field variables then are also dependent on the ratio h/d, d being the film thickness as shown in Fig. 2. However, when the indentation depth is held constant during the test, steady-state conditions prevail, and the global quantities discussed above are constantly facilitating a direct comparison with the corresponding homogeneous solution when warranted.

In the present analysis, as mentioned above, it is assumed that the material behavior is adequately described by classical elastoplasticty or, in a few cases, pressure-sensitive Drucker–Prager plasticity.[35] Despite this, the resulting boundary value problem becomes very involved (in particular, so as a film/substrate boundary is introduced into the problem), and it is necessary to use the FEM to arrive at results of acceptable accuracy. The basic numerical scheme for an analysis of the corresponding homogeneous problem was developed by Wredenberg and Larsson[24,25] and further improved for thin film problems by Larsson and Wredenberg.[32] This scheme will be closely adhered to also in the present investigation and consequently, below, only the most important elements in this numerical approach are discussed with the particular ingredients due to the presence of a film/substrate system described in some detail.

For the constitutive specification, the incremental, rate-independent Prandtl–Reuss equations for classical large deformation von Mises plasticity with isotropic hardening were implemented. At elastic loading, or unloading, a hypoelastic formulation of Hooke's law, pertinent to the elastic part of the Prandtl–Reuss equations, was relied upon. Obviously, within this setting, kinematic hardening effects were not included in the analysis. Such effects can certainly influence the outcome of a scratch test but particularly so during the unloading sequence of the test. In the present analysis, the loading part of the scratch test is of primary interest and for this reason, and also for clarity (the interpretation of the results becomes more involved due to an increased number of constitutive parameters), only isotropic hardening is considered here. For metallic materials, the material strain-hardening (in the plastic deformation region) is described by a standard power law relation according to

$$\sigma(\varepsilon_p) = \sigma_y + \sigma_c \varepsilon_p^{(1/n)}, \tag{2}$$

where $\sigma(\varepsilon_p)$ is the material flow stress, σ_y is the initial yield stress, ε_p is as mentioned above the accumulated plastic strain, and σ_c and n are material constants; in addition, a hardening behavior representative of polymeric materials is considered. In the latter case, as mentioned above, both classic Mises plasticity and a material behavior pertinent to pressure-sensitive flow, here described using the Drucker–Prager[35] material model, are of interest. The pressure sensitivity of such a material is characterized by (together with the standard assumptions in von Mises classical large deformation elastoplasticity) a parameter known as the ''friction angle,'' α, allowing the yield stress to vary with the mean stress, σ_m. The yield surface may then be described in a standard manner as

$$\sigma_e + \tan(\alpha)\sigma_m = \sigma_0. \tag{3}$$

In equation (3), σ_0 is the yield stress at zero mean stress (pure shear), and σ_e is the Mises effective stress. Evidently, the angle α represents the slope of the yield surface in the σ_e vs σ_m stress space. Finally, it should be clearly stated that explicit values on the materials parameters are presented in connection with the discussion of the results in Section 4.

The numerical simulations were performed using FEMs implemented in the commercial FEM package ABAQUS.[37] As the material experienced very large strains, ALE-adaptive meshing was used to maintain the element integrity. In the case of thin film scratching the mesh was composed of approximately 80,000 linear eight-noded elements, which is shown in Fig. 3

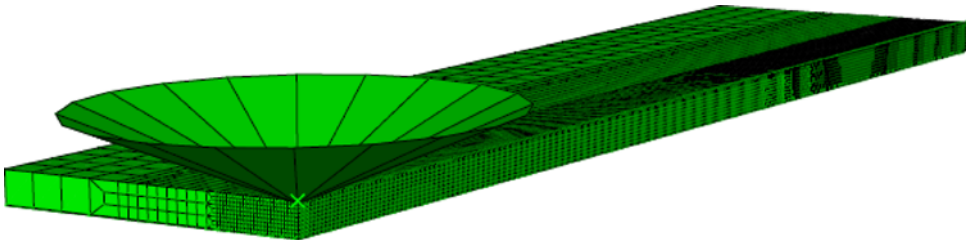

Fig. 3: Finite element mesh with linear 8-node brick elements. Symmetry conditions apply to the right hand surface below the conical stylus

(the corresponding mesh at scratching of monolithic (homogeneous) materials is not shown here for brevity but is presented by, for example, Wredenberg and Larsson[25]). The elements were of hybrid type, i.e., the displacements were approximated with bilinear shape functions while the hydrostatic pressure attained a constant value in each element, to improve convergence at almost incompressible deformation. Linear elements were chosen instead of quadratic elements as they do not show the inherent contact problems of such elements, ABAQUS.[37] It should also be emphasized that the number of elements used in the numerical simulations were not fixed but varied somewhat to ensure that the contact area included as many elements as possible to ensure high accuracy results. As regards to boundary conditions, the surface outside the contact area was assumed traction free, and within the region of contact unilateral kinematic constraints, given by the shape of the rigid, conical indenters were accounted for. In this context, it should be mentioned that loading was applied by prescribing the normal and tangential displacement of the rigid stylus. In order to simulate the film/substrate boundary, zero displacements and rotations were imposed along the lower surface (not shown) of the mesh in Fig. 3. Obviously, as already mentioned above, this corresponds to the case of a soft film on a hard (stiff) substrate with perfect bonding (except, of course, at cracking) along the interface. At monolithic scratching, the outer boundaries of the mesh were chosen to be sufficiently far away from the contact area to avoid any remote boundary effects. This corresponds to scratching of a homogeneous half-space. Finally, it should be mentioned that friction between the indenter and the thin film surface was introduced in some of the calculations by using a standard Coulomb friction model. This will be discussed in detail later.

Delamination analysis

One of the most important reasons for studying the stress fields at thin film scratching concerns the fact that this is essential for understanding the initiation of delamination at scratching. Recently, Wredenberg and Larsson[33,36] used cohesive zone analysis to study delamination initiation and growth at scratching. In this investigation, the load at crack forming and subsequent growth is not of immediate interest but instead, the evolution of the stress fields in such a situation is studied. Consequently, only the most important features of a numerical analysis of delamination at thin film scratching is presented here directly, and for more details we refer to Wredenberg and Larsson.[33,36]

As for the delamination analysis, it is well known that the delamination process can be severely influenced by mode mixity, and for this reason a general energy release rate-based criterion was used according to

$$G = G_c(\psi), \tag{4}$$

as suggested by Hutchinson and Suo[38] for mixed-mode crack propagation along a weak plane. In (4), G_c is the separation energy necessary for the delamination of the film. This energy may then be allowed to vary depending on the mode of crack growth (i.e., mode I, mode II, or a combination thereof). The mode mixity may be described by a parameter ψ,[33] defined as

$$\psi = (2/\pi)\arctan(K_{II}/K_I). \tag{5}$$

In equation (5), K_I and K_{II} are mode I and II stress intensity factors, respectively. Furthermore, to be able to model the creation of a new surface with the accompanying separation energy at delamination of a film/substrate interface numerically, a cohesive zone model was implemented. Commonly, the cohesive laws are defined through an interfacial potential φ with a traction vector $\boldsymbol{T} = (T_n, T_t)$ acting on the cohesive surface[39–41] as

$$T = -\frac{\partial\phi(\Delta)}{\partial\Delta}, \tag{6}$$

where $\Delta = (\Delta_n, \Delta_t)$ indicate the separation of the surfaces. In general, as the cohesive surfaces separate, the traction will increase until a maximum is reached, after which it will decrease to zero, resulting in complete separation. Consequently, the area under the curve is the energy needed for separation.

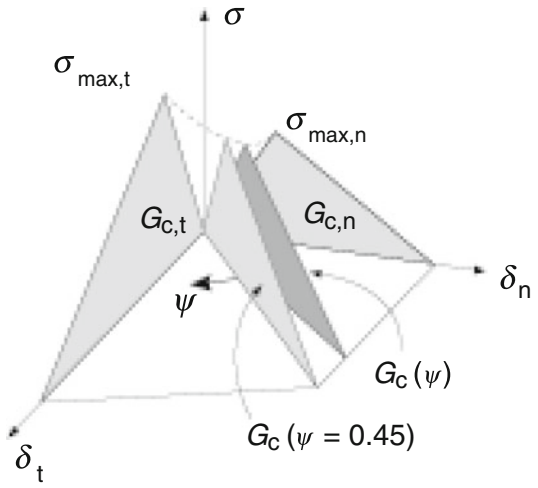

Fig. 4: Sketch of the mixed-mode cohesive law used in the numerical simulations. The critical energy release rate is labeled $G_c(\psi)$ and the maximum traction σ_{max}. δ indicate crack opening. The indices n and t indicate normal and shear, respectively

In the numerical analysis, the adhesive bond between the film and the (rigid) substrate were accounted for using 10,000 cohesive elements with an implemented traction–separation law as shown in Fig. 4. The cohesive law used was defined by five parameters: the maximum cohesive stresses ($\sigma_{max,n}$ and $\sigma_{max,t}$) and the critical energy release rates: (G_c ($\psi = 0$), G_c ($\psi \approx 0.45$), G_c ($\psi = 1$)). The damage initiation criterion (the dashed line in Fig. 4) could be expressed as

$$(\sigma_n/\sigma_{max,n})^2 + (\sigma_t/\sigma_{max,t})^2 = 1, \quad (7)$$

where σ_n and σ_t are the tractions in the normal and shear direction, respectively. It should be emphasized that the explicit values on the five parameters were determined experimentally for a vinyl–ester polymer by Wredenberg and Larsson[33,36] and are used as a representative material also here. Explicit values for the critical energy release rates are shown in Fig. 5 while the cohesive stresses take on the values $\sigma_{max,n} = 21$ and $\sigma_{max,t} = 27$ MPa, respectively.

The cohesive elements were for numerical purposes given an initial stiffness of 30 TPa/m corresponding to the initial slope of the cohesive law. A study of the importance of this parameter on the delamination load was performed, and it was concluded that any of the tested stiffness values from 20 to 80 TPa/m would suffice (the results differed with <0.5%). Ultimately, the stiffness of 30 TPa/m was chosen as it allows reasonably large elements, and thus lower computational times as a stiffer cohesive law requires a denser element mesh.

Delamination was said to occur when some cohesive element experienced more than 99% of accumulative

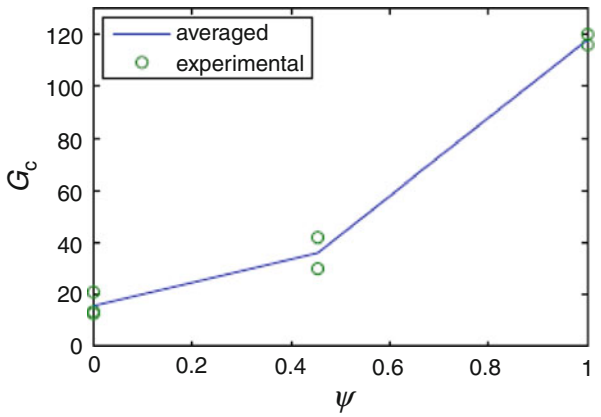

Fig. 5: Results from the critical energy release rate experiments by Wredenberg and Larsson.[33,36] The averaged results are used in the present numerical calculations

damage; meaning that the cohesive deformation had passed the point of maximum traction and that the tractions T were down to 1% of the maximum tractions of an undamaged element. This choice was not of any real importance, but was chosen to avoid any numerical peculiarities involved in the case of a value being 100% accumulated damage. Indeed, changing this value to 100% would cause an indistinguishable change in the simulated delamination load.

Finally, in this context, it should be emphasized once again that a determination of such features as, for example, delamination load and shape was not of immediate interest in the present analysis. Consequently, the explicit values on the cohesive parameters presented above, and used in the numerical simulations, are not of direct importance but should be regarded as being representative for a typical soft polymeric coating.

Results and discussion

The results presented and discussed below concern the mechanical behavior at scratching of thin film/substrate systems. In particular, the stress field variables are of interest to explain in some detail the delamination behavior at thin film scratching, but the results can also give some guidance as regards to such features as, for example, surface cracks and pressure sensitivity. In doing so, it is believed that essentially three field variables are of immediate interest, namely the largest principal stress, the shear stress parallel with the film/substrate interface, and the normal stress perpendicular to the interface. The materials investigated are: (1) a classical elastoplastic material with a hardening behavior pertinent to metals, (2) a classical elastoplastic material with a hardening behavior pertinent to polymers, and (3) the same polymeric material but also accounting for pressure-sensitive flow. Loading was applied by, as mentioned above, prescribing the

displacement of the conical stylus and in particular at scratching of monolithic materials and also film/substrate systems with no delamination present; the normal displacement was held constant to achieve steady-state conditions. On the other hand, in the calculations pertinent to the delamination analysis, the normal indentation depth was continuously increased to initiate crack formation and subsequent growth.

It seems advisable to start the presentation of the results by first investigating the stress-field behavior for a classical metallic homogeneous material, i.e., the case of a monolithic material with no interface present. The constitutive constants pertinent to this material are:

$$\Lambda = 200, \quad \sigma_{\text{rep}} = 210 \text{ MPa}, \quad \nu = 0.3, \tag{8}$$

cf. equation (1), and

$$\sigma_{\text{y}} = 105 \text{ MPa}, \; n = 3, \tag{9}$$

cf. equation (2). The results are shown in Fig. 6 (normal stresses) and in Fig. 7 (shear stress) and it

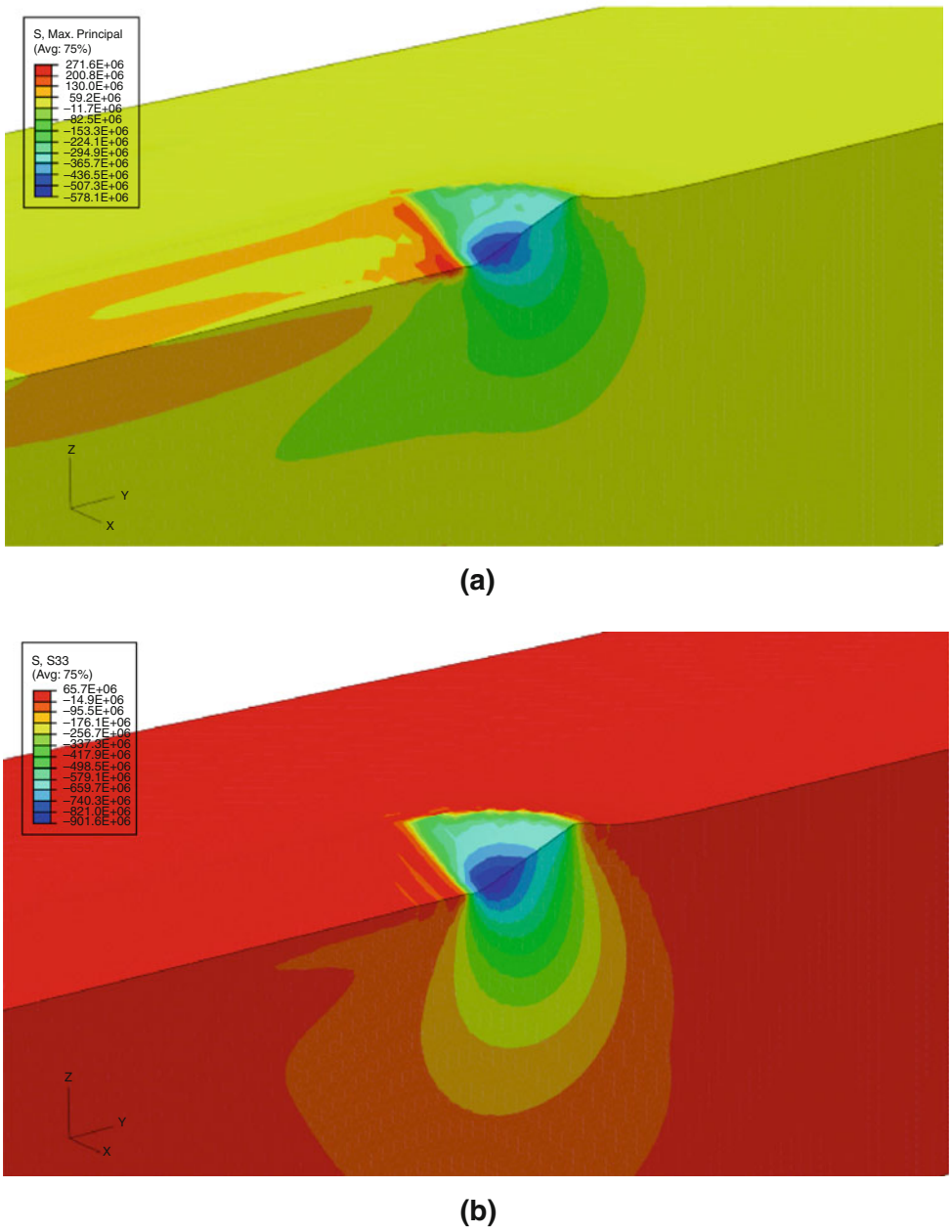

Fig. 6: Normal stress trajectories at monolithic scratching of the metallic material defined in equations (8) and (9). Classical Mises plasticity is assumed. Units in Pa. (a) First principal stress. (b) σ_{33}

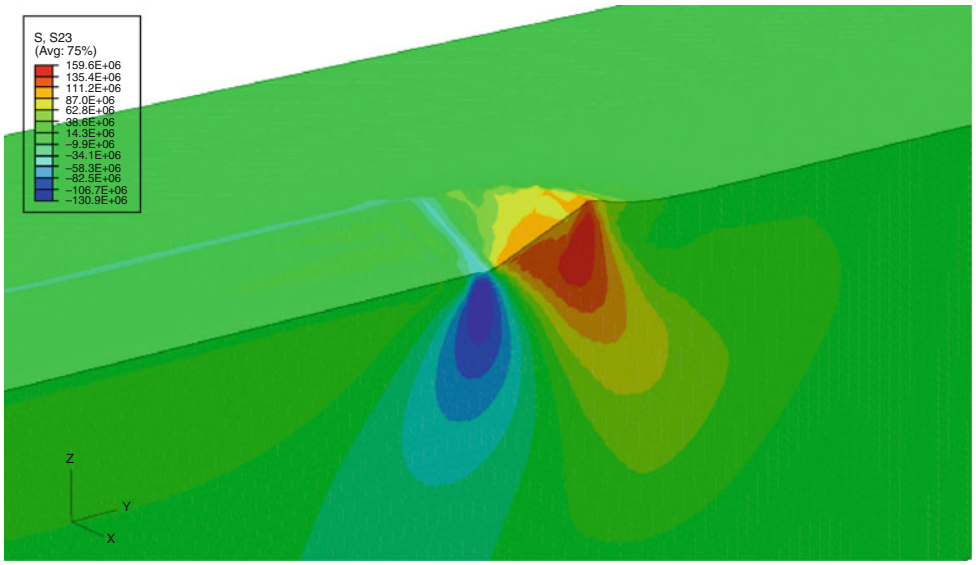

Fig. 7: Shear stress, τ_{23}, trajectories at monolithic scratching of the metallic material defined in equations (8) and (9). Classical Mises plasticity is assumed. Units in Pa

should be immediately emphasized that it is of course of little or no value to evaluate these results in connection with delamination growth; instead, they should mainly serve as a guideline as to how the interface influences the different stress field variables. As regards to the monolithic results, it is clear that the normal stress components are essentially compressive and tensile values are present only at the wake of the stylus (and only when the largest principal stress is concerned). Furthermore, to be remembered in the forthcoming discussion below, it should be noted that the shear stress τ_{23} (acting parallel with the interface) attains high values all over and also well below the contact area.

In Figs. 8 and 9, the corresponding results in the case of a film/substrate interface being present, for the same material as in Figs. 6 and 7, is shown. The ratio *h/d* takes on the value 0.5, and subsequently, the interaction between contact and interface is substantial. As is evident from the results in Figs. 8 and 9, the main conclusion from the monolithic analysis remains, i.e., shear stresses are high and normal stresses are predominantly compressive. Regarding details it can be observed that the shear stresses in Fig. 9 are even higher than at scratching of monolithic materials and that the highest values are present at, and close to, the interface. Furthermore, owing to interface effects, there is also an area of tensile normal stresses developing in front of the stylus below the surface extending down to the interface; but, in short, these tensile stresses are low. For clarity, frictional effects were not included in these initial calculations presented in Figs. 6–9.

The results above are, as emphasized previously, pertinent to a metallic material. For the particular situation analyzed here, a soft film on a hard substrate, this is perhaps not of most immediate interest, but is included for completeness. Instead, polymeric films are a more natural class of materials to analyze in this context. In doing so, a vinyl–ester material, exhibiting both softening and hardening after initial yield, previously characterized by Wredenberg and Larsson,[33,36] was singled out for attention. The material properties for this material are

$$E = 3.5\ \text{GPa},\ \nu = 0.5,\ \Lambda = 21, \tag{10}$$

and the behavior after initial yielding is shown in Fig. 10. It should also be mentioned that, as pointed out by Wredenberg and Larsson,[33,36] as the hardening region in Fig. 10 could not be well described due to cracking and barrelling during uniaxial testing, this feature was not included in the numerical simulations. In addition to this, it should be mentioned that frictional effect was for completeness included in the analysis of the polymeric film discussed below. In doing so, standard Coulomb friction was assumed with the adhesive component of the coefficient of friction being

$$\mu = 0.07, \tag{11}$$

cf. e.g., Wredenberg and Larsson,[33] representative of this type of polymer. It should be noted in passing in this context that both local and global scratch properties are very much dependent of frictional effects. This is in contrast to the situation at normal indentation as then at least global parameters such as hardness are almost independent of friction.[42]

Accordingly then, stress field trajectories for scratching of the polymeric film/substrate system, with no delamination present, are shown in Fig. 11 (normal stresses) and in Fig. 12 (shear stress). The corresponding

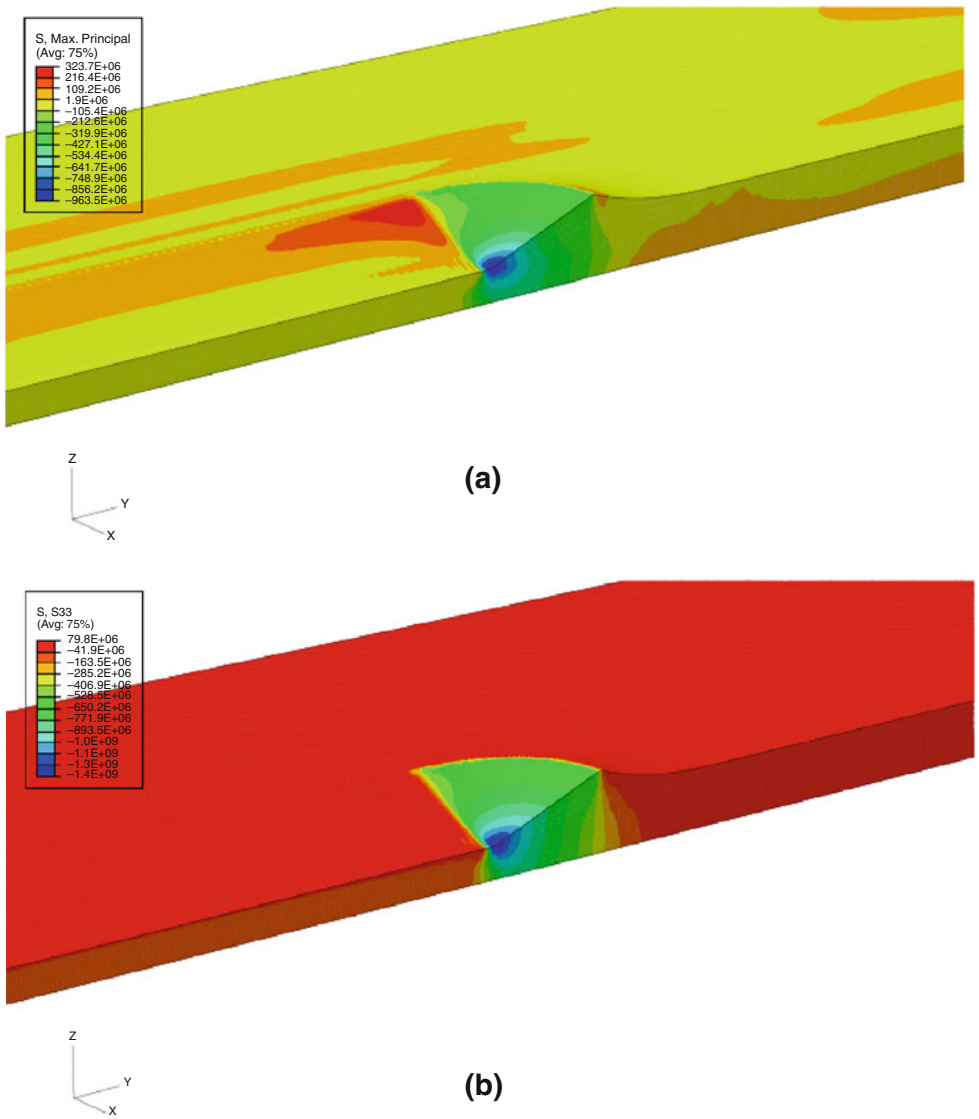

Fig. 8: Normal stress trajectories at thin film scratching of the metallic material defined in equations (8) and (9). The ratio *h/d* takes on the value 0.5. Classical Mises plasticity is assumed. Units in Pa. (a) First principal stress. (b) σ_{33}

results for the metallic film have already been presented, in Figs. 8 and 9, and discussed, and obviously, these two sets of results show similar behavior. Consequently, normal stresses are mainly compressive with very small regions of high tensile values and shear stresses, especially so at the film/substrate interface. The stress values in Figs. 11 and 12 are lower than corresponding metallic ones; in this case, the ratio *h/d* takes on the value 0.28 so that the two sets of results are comparable, but this is of course almost self-evident remembering the difference in, for one thing, the different stress levels in the plastic region. There are also some differences between the two sets of results as regards to the shape of the stress trajectories, but this is immediately explained by the fact that friction is accounted for in the polymeric case. It should also be mentioned that a higher value on the ratio *h/d* will increase the explicit values on the stresses. This is due to the ''capturing'' effect of the material between the stylus and the rigid substrate and will accordingly enhance the probability of coating delamination.

Based on the results in Figs. 8 and 9 and in Figs. 11 and 12, it seems appropriate to suggest that the high shear stress values at the film/substrate interface are the driving forces for the initiation of delamination. In order to achieve further understanding of the delamination process in combination with the related stress fields, it is of course also important to investigate the situation at progressing crack growth. This is done presently by studying delaminated areas of different size (the delamination size is related to a representative length of the contact region, for example $\sqrt{A}$). Only the polymer defined in equation (10) and in

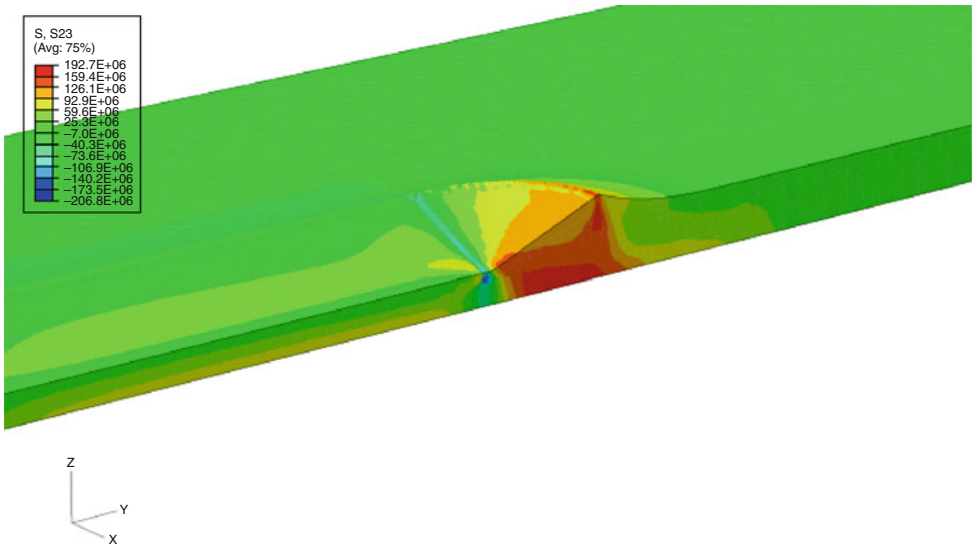

Fig. 9: Shear stress, τ_{23}, trajectories at thin film scratching of the metallic material defined in equations (8) and (9). The ratio *h/d* takes on the value 0.5. Classical Mises plasticity is assumed. Units in Pa

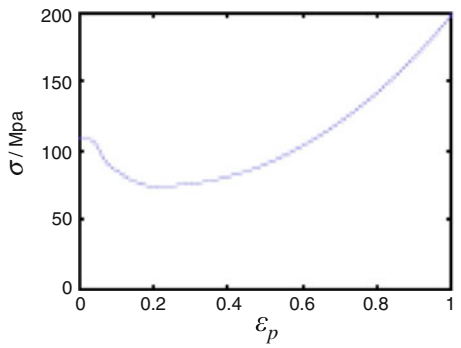

Fig. 10: Typical stress–strain (ε_p) curve of the presently analyzed polymeric material. Determined by Wredenberg and Larsson[33,36]

Fig. 10 is considered here, and explicit results are only discussed and not shown for brevity. In the case of a small initial delamination, it was noticed that the maximum values of the shear stress are no longer present along the interface but can be found inside the film. This is partly due to the fact that a new surface is created at delamination but it is also a consequence of the fact that delamination occurs at relatively small values on the indentation depth, i.e., $h/d < 0.28$ (being the indentation depth in Figs. 11 and 12). Normal stresses remain compressive. At increasing load, the delaminated area will continue to grow, but the results from the simulations indicate that the stresses are not significantly influenced by this feature. Regarding details, the shear stresses are slightly decreased at delamination growth which is somewhat surprising as the applied load (acting on the stylus) is larger in this case. This clearly indicates that delamination growth at scratching is a stable process, and a continuously increased load is required in order to prevent crack arrest. However, a more detailed investigation of this matter is left for future studies.

From the results presented above, it can accordingly be concluded that both delamination initiation and growth at thin film scratching are driven by high values on shear stresses. This conclusion was also suggested by Wredenberg and Larsson,[33] based on an analysis of relevant cohesive zone crack parameters, but is here confirmed from the evolution of the stress field in such a situation. It may be appropriate to mention here that in none of the simulations performed did the delamination initiate anywhere except in front of the stylus where the shear stresses are at their highest. There is, however, also other important information that can be retrieved from the present detailed study of the stresses at scratching. One such feature concerns the initiation of cracking away from the interface. The most obvious cracking system that can be noted based on the stress fields presented above then concerns cracking in the wake of the stylus. This is so at scratching of thin film as well as homogeneous materials, and for both the metal and the polymer. Cracks in the wake of the stylus have been observed experimentally by, for example, Browning et al.[43] and Holmberg et al.,[44] which is immediately explained by the stress trajectories shown above (Figs. 6–9, 11 and 12). Although coating defects were not included in this investigation, it may be argued that a sufficiently large pre-existing crack in the coating must cause a significant disturbance in the stress field compared to the ideal case. Most likely, at some point, this will result in a stress concentration in the coating substrate interface (or propagation causing large-scale fracture/delamination). In particular, in the case of surface cracks, these might grow due to the tensile stresses formed in the wake of the stylus. Along the same line, any defect in the interface weakening the bond prior to scratching could certainly increase

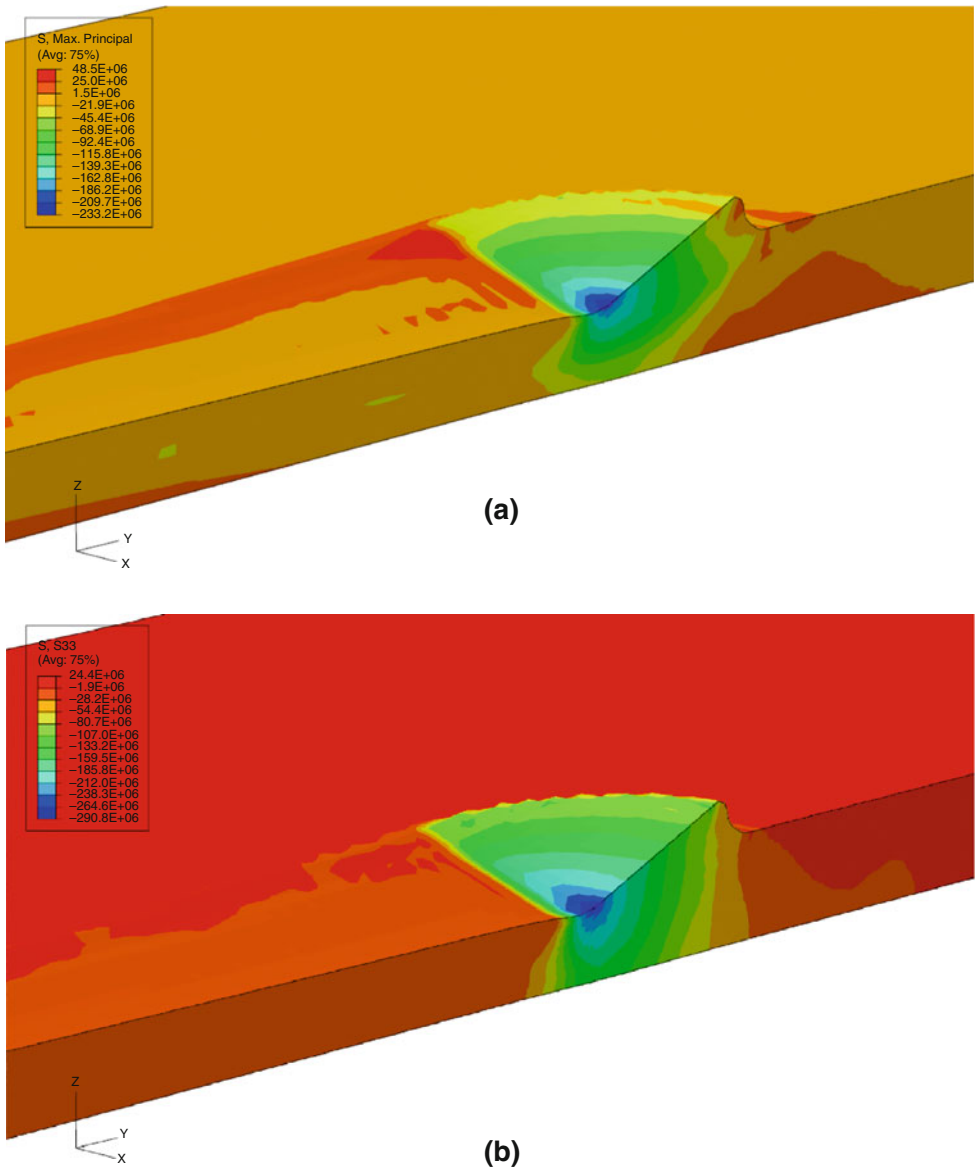

Fig. 11: Normal stress trajectories at thin film scratching of the polymeric material defined in equation (10) and Fig. 13. The ratio *h/d* takes on the value 0.28. Classical Mises plasticity is assumed. Units in Pa. (a) First principal stress. (b) σ_{33}

the probability of delamination growth ahead of the stylus in the region of high shear stresses.

Another matter of importance in the present situation concerns the behavior of the stress fields at pressure-sensitive constitutive behavior. This is of importance particularly for polymeric films, and related matters concerning crack behavior have been studied previously,[33,36] but not in the context of stress-field behavior. In doing so, the polymer analyzed above was assumed to behave as a pressure-sensitive material, described by the Drucker–Prager[35] material model, with a rather high value (to clarify relevant features) on the ''friction angle,'' α, in equation (3):

$$\alpha = 8^{\circ}. \tag{12}$$

Thin film results for the stress field in this case (no delamination is present) is shown in Figs. 13 and 14 and should be compared to the corresponding ones in Figs. 11 and 12, where standard Mises plasticity is assumed. The scratch depth is slightly lower in this case though; h/d takes on the value 0.17. It is clear from this comparison that pressure-sensitivity effects are very small as regards to the stress levels involved. Also the shapes of the trajectories are similar even though some difference between the two sets of results was found for, in particular, the shear stress. However, this difference can be immediately explained by the fact that the indentation depth in Figs. 13 and 14 is smaller than the one in Figs. 11 and 12. Accordingly, it can be concluded based on the behavior of the relevant stress

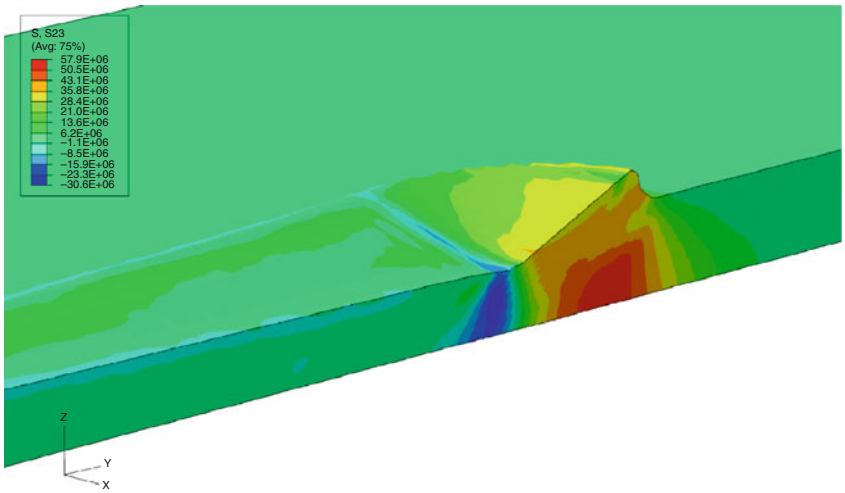

Fig. 12: Shear stress, τ_{23}, trajectories at thin film scratching of the polymeric material defined in equation (10) and Fig. 13. The ratio *h/d* takes on the value 0.28. Classical Mises plasticity is assumed. Units in Pa

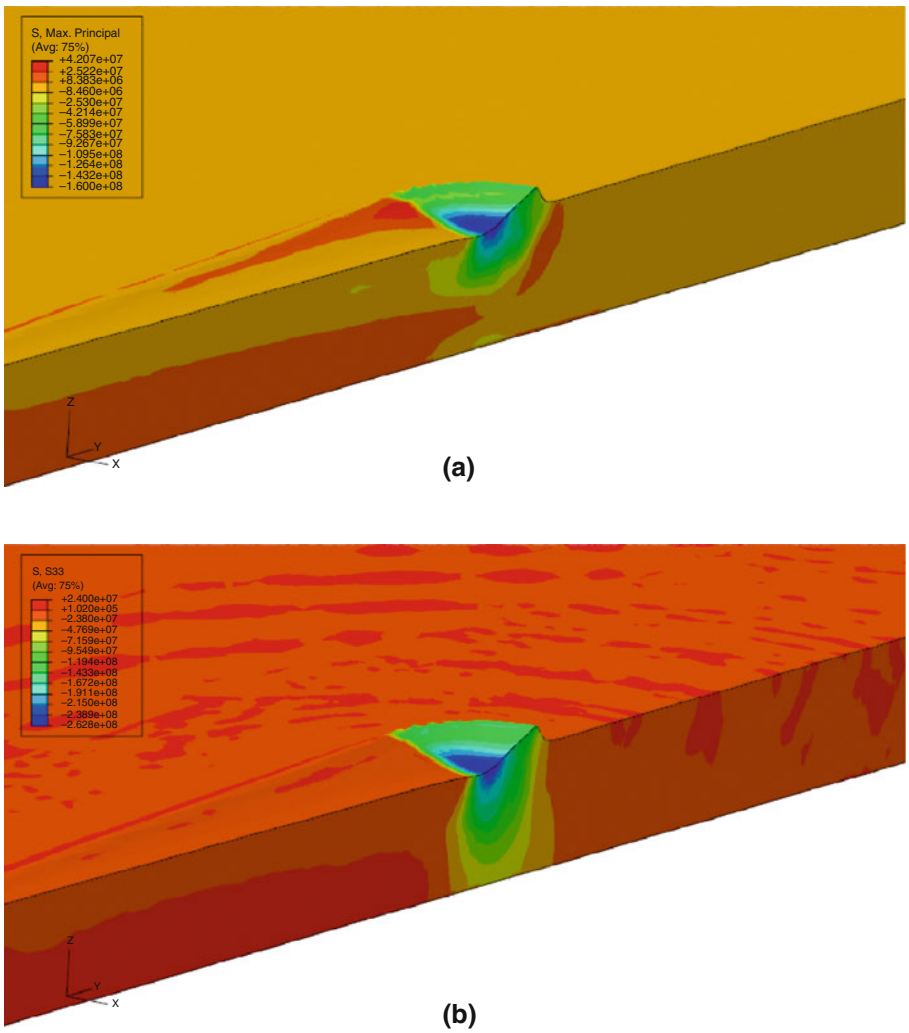

Fig. 13: Normal stress trajectories at thin film scratching of the polymeric material defined in equations (10), (12), and Fig. 13. The ratio *h/d* takes on the value 0.17. Drucker–Prager[33] pressure-sensitive plasticity is assumed. Units in Pa. (a) First principal stress. (b) σ_{33}

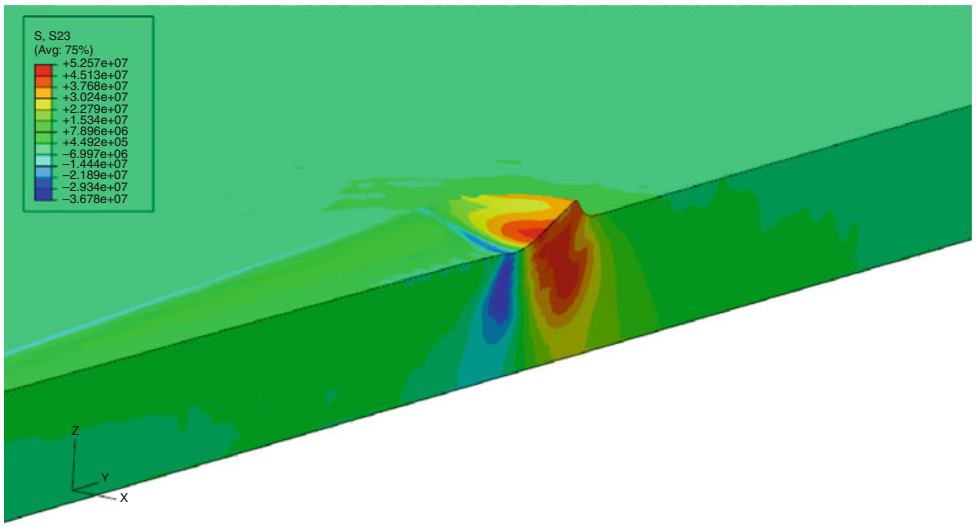

Fig. 14: Shear stress, τ_{23}, trajectories at thin film scratching of the polymeric material defined in equations (10), (12), and Fig. 13. The ratio *h/d* takes on the value 0.17. Drucker–Prager[33] pressure-sensitive plasticity is assumed. Units in Pa

fields that pressure-sensitive flow will have a small effect on, for example, the delamination load. The same conclusion was presented by Wredenberg and Larsson[33,36] based on a fracture mechanics approach.

As a final comment, it should be emphasized once again that in the present study, crack initiation and growth were introduced into the problem by using cohesive zone analysis. It deserves to mention that a direct attack on the delamination problem based on linear fracture mechanics, in the spirit of, for example, Nilsson et al.[45] or Larsson,[46] is of course also a possible, but indeed a less accurate alternative as it requires some assumption about the shape of the initial delamination.

Conclusions

Scratching of thin film/substrate systems was analyzed numerically in order to determine the behavior of relevant stress fields in such a situation. The correlation of this behavior with different features at scratching is discussed in some detail. The investigation was focused on the situation where the thin film is considerably softer than the substrate. The most important qualitative findings given by the numerical results can be summarized as follows:

- High shear stresses are the driving force for delamination initiation and growth along the film/substrate interface.
- High tensile stresses are only found in the wake of the stylus possibly leading to cracking in this region.
- The influence from pressure-sensitive flow on the stress fields related to delamination initiation is small, both quantitatively and qualitatively.

Acknowledgments The authors acknowledge the support through Grant 621-2005-5803 from the Swedish Research Council.

References

1. Sneddon, IN, "The Relation Between Load and Penetration in the Axisymmetric Boussinesq Problem for a Punch of Arbitrary Profile." *Int. J. Eng. Sci.*, **3** 47–57 (1965)
2. Tabor, D, *Hardness of Metals*. Oxford University Press, Oxford, UK (1951)
3. Johnson, KL, "The Correlation of Indentation Experiments." *J. Mech. Phys. Solids*, **18** 115–126 (1970)
4. Oliver WC, Pharr GM, "An Improved Technique for Determining Hardness and Elastic-Modulus Using Load and Displacement Sensing Indentation Experiments." *J. Mater. Res.*, **7** 1564–1583 (1992)
5. Cheng YT, Cheng CM, "Scaling, Dimensional Analysis and Indentation Measurements." *Mater. Sci. Eng. R Rep.*, **44** 91–149 (2004)
6. Bhattachharya, AK, Nix, WD, "Finite Element Simulation of Indentation Experiments." *Int. J. Solids Struct.*, **24** 881–891 (1988)
7. Bhattachharya, AK, Nix, WD, "Analysis of Elastic and Plastic Deformation Associated with Indentation Testing of Thin Films on Substrates." *Int. J. Solids Struct.*, **24** 1287–1298 (1988)
8. Laursen, TA, Simo, JC, "A Study of the Mechanics of Microindentation Using Finite Elements." *J. Mater. Res.*, **7** 618–626 (1992)
9. Giannakopoulos, AE, Larsson, PL, Vestergaard, R, "Analysis of Vickers Indentation." *Int. J. Solids Struct.*, **31** 2679–2708 (1994)
10. Larsson, PL, Giannakopoulos, AE, Söderlund, E, Rowcliffe, DJ, Vestergaard, R, "Analysis of Berkovich Indentation." *Int. J. Solids Struct.*, **33** 221–248 (1996)
11. Giannakopoulos, AE, Larsson, PL, "Analysis of Pyramid Indentation of Pressure-Sensitive Hard Metals and Ceramics." *Mech. Mater.*, **25** 1–35 (1997)

12. Larsson, PL, Giannakopoulos, AE, ''Tensile Stresses and Their Implication to Cracking at Pyramid Indentation of Pressure-Sensitive Hard Metals and Ceramics.'' *Mater. Sci. Eng. A*, **254** 268–281 (1998)
13. Wang, HF, Yang, X, Bangert, H, Torzicky, P, Wen, L, ''Two-Dimensional FEM Simulation of Vickers Indentation of Hardness Measurements.'' *Thin Solid Films*, **214** 68–73 (1992)
14. Cai, X, Bangert, H, ''Hardness Measurements of Thin Films: Determining the Critical Ratio of Depth to Thickness Using FEM.'' *Thin Solid Films*, **264** 59–71 (1995)
15. Sun, Y, Bell, T, Zheng, S, ''Finite-Element Analysis of the Critical Ratio of Coating Thickness to Indentation Depth for Coating Property Measurements by Nanoindentation.'' *Thin Solid Films*, **258** 198–204 (1995)
16. Knapp, JA, Follstaed, DM, Myers, SM, Barbour, JC, Friedmann, TA, ''Finite-Element Modeling of Nanoindentaion.'' *J. Appl. Phys.*, **85** 1460–1474 (1999)
17. Larsson, PL, Peterson, IRM, ''Evaluation of Sharp Indentation Testing of Thin Films and Ribbons on Hard Substrate.'' *J. Test. Eval.*, **30** 64–73 (2002)
18. Pethica, JB, Hutchings, R, Oliver, WC, ''Hardness Measurements at Penetration Depths as Small as 20 nm.'' *Philos. Mag. A*, **48** 593–606 (1983)
19. Goddard, J, Wilman, H, ''A Theory of Friction and Wear During the Abrasion of Metals.'' *Wear*, **5** 114–135 (1962)
20. Childs, THC, ''The Sliding of Rigid Cones Over Metals in High Adhesion Conditions.'' *Int. J. Mech. Sci.*, **12** 393–403 (1970)
21. De Vathaire, M, Delamare, F, Felder, E, ''An Upper Bound Model of Ploughing by a Pyramidal Indenter.'' *Wear*, **66** 55–64 (1981)
22. Gilormini, P, Felder, E, ''Theoretical and Experimental Study of the Ploughing of a Rigid-Plastic Semi-Infinite Body by a Rigid Pyramidal Indenter.'' *Wear*, **88** 195–206 (1983)
23. Bucaille, JL, Felder, E, Hochstetter, G, ''Mechanical Analysis of the Scratch Test on Elastic and Perfectly Plastic Materials with Three-Dimensional Finite Element Modeling.'' *Wear*, **249** 422–432 (2001)
24. Wredenberg, F, Larsson, PL, ''On the Numerics and Correlation of Scratch Testing.'' *J. Mech. Mater. Struct.*, **2** 573–594 (2007)
25. Wredenberg, F, Larsson, PL, ''Scratch Testing of Metals and Polymers—Experiments and Numerics.'' *Wear*, **266** 76–83 (2009)
26. Bull, SJ, ''Failure Modes in Scratch Adhesion Testing.'' *Surf. Coat. Technol.*, **50** 25–32 (1991)
27. Frey, N, Mettraux, P, Zambelli, G, Landolt, D, ''Modified Scratch Test for Study of the Adhesion of Ductile Coatings.'' *Surf. Coat. Technol.*, **63** 167–172 (1993)
28. Thouless, MD, ''An Analysis of Spalling in the Microscratch Test.'' *Eng. Fract. Mech.*, **61** 75–81 (1998)
29. Malzbender, J, de With, G, ''Scratch Testing of Hybrid Coatings of Float Glass.'' *Surf. Coat. Technol.*, **135** 202–207 (2001)
30. Yueguang, W, Manhong, Z, Shan, T, ''Characterization of the Fracture Work for Ductile film Undergoing the Micro-Scratch.'' *Acta Mech. Sin.*, **18** 494–505 (2002)
31. Holmberg, K, Laukkanen, A, Ronkainen, H, Wallin, K, Varjus, S, ''A Model for Stresses, Crack Generation and Fracture Toughness Calculation in Scratched Tin-Coated Steel Surfaces.'' *Wear*, **254** 278–291 (2003)
32. Larsson, PL, Wredenberg, F, ''On Indentation and Scratching of Thin Films on Hard Substrates.'' *J. Phys. D Appl. Phys.*, **41** 074022 (2008)
33. Wredenberg, F, Larsson, PL, ''Delamination of Thin Coatings at Scratching—Experiments and Numerics.'' *J. Mech. Mater. Struct.*, **4** 1041–1062 (2009)
34. Wredenberg, F, Larsson, PL, ''On the Effect of Substrate Deformation at Scratching of Soft Thin Film Composites.'' Report, KTH Solid Mechanics, 10044, Stockholm, Sweden, 2008, submitted for international publication
35. Drucker, DC, Prager, W, ''Soil Mechanics and Plastic Analysis or Limit Design.'' *Quart. Appl. Mech.*, **10** 157–162 (1952)
36. Wredenberg, F, Larsson, PL. ''On Scratch Testing of Pressure-Sensitive Polymeric Coatings.'' *J. Coat. Technol. Res*., 2009. doi: 10.1007/s11998-009-9202-4
37. ABAQUS. *ABAQUS Manual v.6.7*. Hibbit, Karlsson & Sorensen, Inc., Pawtucket, RI (2008)
38. Hutchinson, JW, Suo, Z, ''Mixed Mode Cracking in Layered Materials.'' *Adv. Appl. Mech.*, **29** 63–191 (1992)
39. Xu, XP, Needleman, A, ''Numerical Simulations of Fast Crack Growth in Brittle Solids.'' *J. Mech. Phys. Solid*, **42** 1397–1434 (1994)
40. Needleman, A, ''A Continuum Model for Void Nucleation by Inclusion Debonding.'' *J. Appl. Mech.*, **54** 523–531 (1990)
41. Ortiz, MA, Pandolfi, A, ''Finite-Deformation Irreversible Cohesive Elements for Three-Dimensional Crack-Propagation Analysis.'' *Int. J. Numer. Methods Eng.*, **44** 1267–1282 (1999)
42. Carlsson, S, Biwa, S, Larsson, PL, ''On Frictional Effects at Inelastic Contact Between Spherical Bodies.'' *Int. J. Mech. Sci.*, **42** 107–128 (2000)
43. Browning, RL, Lim, GT, Moyse, A, Sue, HJ, Chen, H, Earls, JD, ''Quantitative Evaluation of Scratch Resistance of Polymeric Coatings Based on a Standardized Progressive Load Scratch Test.'' *Surf. Coat. Technol.*, **201** 2970–2976 (2006)
44. Holmberg, K, Laukkanen, A, Ronkainen, H, Wallin, K, ''Tribological Analysis of Fracture Conditions in Thin Surface Coatings by 3D FEM Modeling and Stress Simulations.'' *Tribol. Int.*, **38** 1035–1049 (2005)
45. Nilsson, KF, Thesken, JC, Sindelar, P, Giannakopoulos, AE, Storåkers, B, ''A Theoretical and Experimental Investigation of Buckling Induced Delamination Growth.'' *J. Mech. Phys. Solids*, **41** 749–782 (1993)
46. Larsson, PL, ''On Delamination Buckling and Growth in Circular and Annular Orthotropic Plates.'' *Int. J. Solids Struct.*, **27** 15–28 (1991)